Finding Seamounts with Altimetry-Derived Gravity Data

Seung-Sep Kim
Dept. of Geology and Earth Environmental Sciences
Chungnam National University
Daejeon, South Korea
seungsep@cnu.ac.kr

Paul Wessel
Dept. of Geology and Geophysics
SOEST, University of Hawaii at Manoa
Honolulu, HI, USA
pwessel@hawaii.edu

***Abstract*—Seamounts are ubiquitous manifestations of underwater volcanism that rise above the surrounding ocean floor by more than a few hundred or thousand meters. Any temporal and spatial variations of the underwater volcanic and tectonic processes that formed seamounts can primarily be understood through their geometric characterization and spatial distribution. For this study, we utilize the vertical gravity gradient (VGG) version 23.1 derived from satellite altimetry, which includes new data from the CryoSat-2, Envisat, and Jason-1 missions. A repeated statistical comparison for an area with no significant geologic features shows that the standard deviation of VGG 23.1 is decreased about 48% from the previous release, indicating the signal-to-noise ratio has been improved significantly from the previous version. In order to examine whether the new data give us better opportunities to find seamounts, we choose near-ridge environments constrained by good bathymetry coverage. For a given area, the nonlinear inversion method to search for seamounts is applied. We approximate VGG anomalies over seamounts as sums of individual, partially overlapping, elliptical polynomial functions, which allows us to form a non-linear inverse problem by fitting the polynomial model to the observations. Model parameters for a potential seamount include geographical location, peak VGG amplitude, major and minor axes of the elliptical base, and the azimuth of the major axis. The non-linear inversion is very sensitive to the initial values for the location and amplitude; hence, they are constrained by the center and amplitude of the uppermost contours obtained with a 1-Eotvos contour interval. With these initial conditions from contouring, we execute a step-wise and fully automated inversion and obtain optimal model estimates for potential seamounts; these are statistically evaluated for significance using the Akaike Information Criterion and *F* tests. Here we present a preliminary result of seamount detection using the new global data and discuss possibilities for constructing a new synthesized global dataset of seamounts.**

Keywords—seamount; altimetry; data analysis; underwater volcanism; statistics

I. Introduction

Seamounts are ubiquitous manifestations of underwater volcanism that rise above the surrounding ocean floor by more than a few hundred or thousand meters [1, 2]. Any temporal and spatial variations of the underwater volcanic and tectonic processes that formed seamounts can primarily be understood through their geometric characterization and spatial distribution [3]. The most uniform global bathymetry data for the ocean basins are derived from satellite altimetry that measures sea surface heights [4]. As the sea surface approximates the geoid, reflecting the mass distribution of sea floor relief, processing of satellite altimetry measurements recovers the anomalous gravity signals over seamounts [5].

Recently the resolution and accuracy of altimetry-derived gravity data are significantly improved by including new non-repeat data of CryoSat-2, Envisat, and Jason-1 missions [4]. Thus, in this study, we first compare the newly released data with the previous version, 16.1, using auto-covariance estimates. Then, to examine whether the new data gives us better opportunity to find small seamounts, we choose near-ridge environments constrained by good bathymetry coverage and apply the non-linear inversion-based seamount searching method. Here we present a preliminary result of seamount detection using the new global data and discuss possibilities to construct new synthesized global dataset of seamounts.

II. Method

A. Vertical Gravity Gradient

The vertical gravity gradient (VGG) grid is the geo-potential data derived from satellite altimetry using a simple algebraic computation that requires neither spherical harmonics nor Fourier transforms [6]. Inherently VGG data amplify short-wavelength signals (e.g., observed over seamounts and fracture zones) and suppress long-wavelength trends (e.g., associated with flexure and hotspot swells). Thus, the VGG grid is more suitable than the free-air gravity (FAA) data for characterizing small underwater features such as seamounts [3]. Fig. 1 shows that gravity anomalies over two small seamounts (4 km apart and 1 km tall) decay when the regional depth increases, while the VGG signals are separable for these two closely located seamounts. In addition, the recently released VGG grid has improved significantly both accuracy and resolution of the data by including new non-repeat altimeter data sets from CryoSat-2, Envisat and Jason-1 missions [4]. This new data should significantly improve our chances of finding unmapped small seamounts, especially those taller than 1 km. Therefore, we have utilized the 1-min Mercator VGG grid to examine if such outcomes are achievable.

This study was supported by the Basic Science Research Program through National Research Foundation (NRF-2013R1A1A1076071) funded by the Ministry of Science, ICT & Future Planning, South Korea.

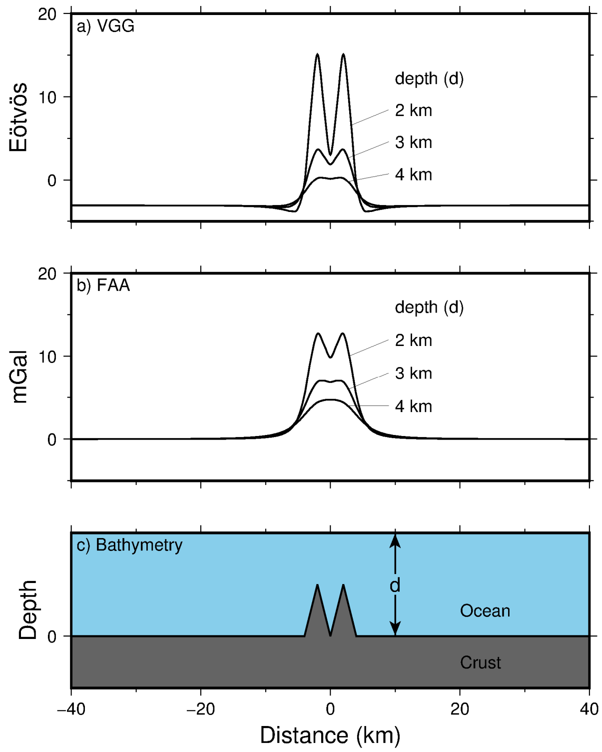

Fig. 1. Limitation of topographic separation from gravity over closely spaced small seamounts. Two 1-km tall seamounts that are 4 km apart are considered for variable depths. While the gravity anomalies over the seamounts become indistinct when the regional depth exceeds the size of seamounts, the vertical gravity gradient anomalies stay separable. Modified from [16].

To compare the newly VGG data with the previous version, 16.1, we applied the indirect method of computing auto-covariance estimates based on the Wiener–Khinchin theorem [7] to an area, where no significant geologic features were observed (Fig. 2). The 2-D auto-covariance estimates were averaged over one radial pixel distance (i.e. the distance between two neighboring grid points of the VGG data in the Mercator domain) to define the correlation length of the VGG data using the first zero-crossing of the radial covariance estimates. The radial auto-covariance estimates indicate that a VGG value at one grid node is strongly correlated with neighboring VGG values located within a radius of 5 pixels for VGG 16.1. However, for VGG 23.1, the first zero-crossing could not be evaluated because of the flat trend of the tail. Instead, the correlation length of VGG 23.1 was estimated at 10% of the normalized covariance, which is above the noise floor. Although the correlation length of the new data appears to be similar to that of the old, the standard deviation of VGG 23.1 is decreased about 48% from the previous release, indicating the signal-to-noise ratio has been significantly improved from the previous. This analysis illustrates that independent multi altimetry data sets are essential to enhance resolving power of the retrieved gravity data and hence can provide better opportunities to reveal unmapped underwater features. Thus, the AltiKa project developed by the Centre National d'Etudes Spatiales (CNES), France, is expected to play another pivotal role to bring up a new opportunity for improving marine gravity.

B. *Characterization of VGG Seamounts*

Morphology of seamounts is diversified, ranging from simple circular, truncated cones to complicated stellate shapes [8]. While large seamounts (h $\geqslant$ 3 km) are often reshaped by the development of rift zones and flank collapses that result in complex volcanic edifices (e.g. Ojin and Nintoku seamounts of the Emperor Seamount Chain [9]), small (h < 1 km) and intermediate (1 $\leqslant$ h < 3 km) seamounts tend to have single volcanic centers and display sub-circular structures (e.g. Lamont Seamount Chain south of the Clipperton Transform [10]).

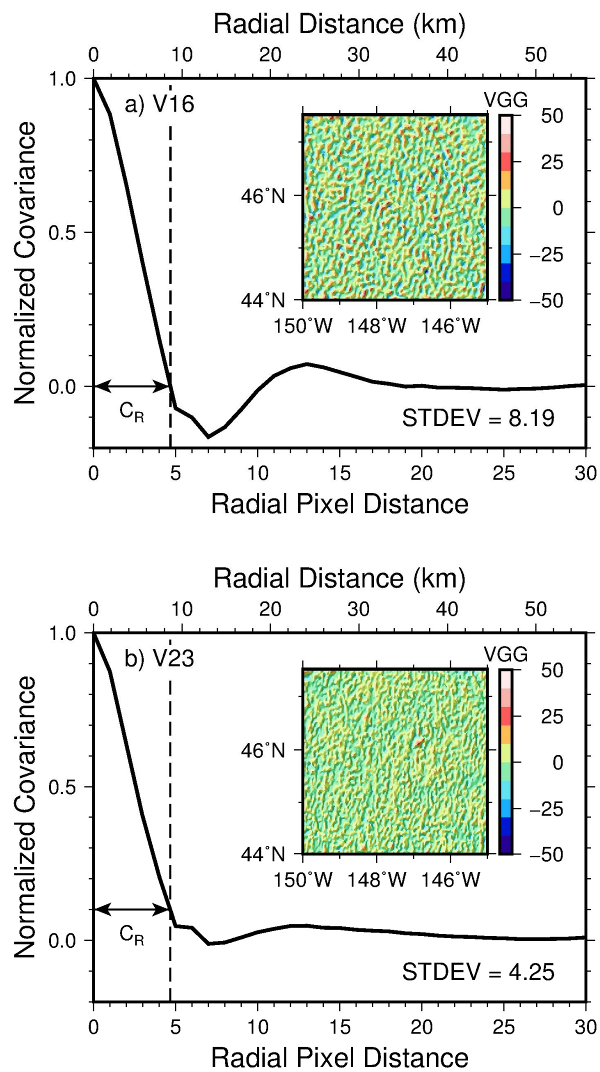

Fig. 2. Radial covariance estimate of the VGG grid at ~45˚N (inset). a) The VGG 16.1 grid has a mean of 0.1 Eötvös and a standard deviation of 8.19 Eötvös. b) The VGG 23.1 grid has a mean of -0.2 Eötvös and a standard deviation of 4.25 Eötvös. Correlation pixel length, C_R, is the distance to the first zero crossing of the covariance estimates.

Previous global seamount studies consistently show that the majority of the detected potential seamounts are smaller than 3 km height [3]. Thus, we can assume an "ideal" volcanic edifice as a simple body, whose VGG responses then can be approximated by an elliptical polynomial model, R, which is similar to the Gaussian model but explicitly goes to zero at the seamount base:

$$R(\mathbf{x},\mathbf{x_o},p,a,b,\theta)=\begin{cases} p\dfrac{(1+r)^3(1-r)^3}{1+r^2}, & |r|\le 1 \\ 0, & |r|>1 \end{cases} \tag{1}$$

Here, $\mathbf{x} = (x, y)$ is the position vector, $\mathbf{x_o} = (x_o, y_o)$ is the summit location, and p is the peak amplitude. Then, the normalized radial distance from the summit, r, is defined as

$$r=\sqrt{A(x-x_o)^2-2B(x-x_o)(y-y_o)+C(y-y_o)^2} \tag{2}$$

with

$$\begin{aligned} A&=\frac{1}{b^2}(f^2\cos^2\theta+\sin^2\theta) \\ B&=\frac{1}{b^2}(1-f^2)\cos\theta\sin\theta \\ C&=\frac{1}{b^2}(f^2\sin^2\theta+\cos^2\theta) \end{aligned} \tag{3}$$

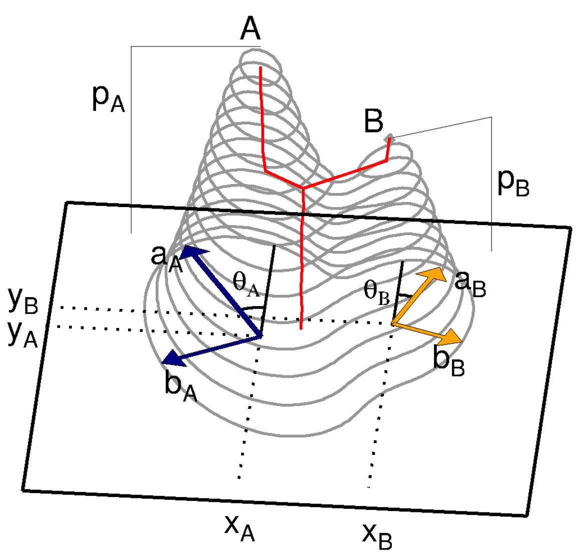

Fig. 3. Schematic diagram of contouring when two VGG potential seamounts with different amplitudes are considered. The model parameters are denoted for the potential seamounts, A and B.

Here, $f = b/a$, where a and b are the major and minor semi-axes of the basal ellipse, respectively, and θ is the angle between the major and east-west (x) axes (Fig. 3). A circular polynomial seamount can be simplified further with

$$r=\frac{\sqrt{(x-x_o)^2+(y-y_o)^2}}{r_o} \tag{4}$$

where r_o is the radius of the seamount base.

If a given domain has S elliptical polynomial seamounts, we can construct a nonlinear least-squares problem for estimating the six parameters, $\mathbf{m} = (p, x_o, y_o, a, b, \theta)$, for each polynomial seamount by minimizing

$$E(\mathbf{M}_S)=\sum_{i=1}^{N}\left[\frac{V_i-R_i(\mathbf{M}_S)}{\sigma_i}\right]^2-2\gamma\sum_{j=1}^{S}\ln p_j \tag{5}$$

where N is the number of data points used for the fit, V_i is the observed VGG at the ith data point, and σ_i its standard deviation of data noise. Here, R_i is the predicted VGG at the ith data point using $\mathbf{M}_S = (\mathbf{m}_1, \mathbf{m}_2, \ldots, \mathbf{m}_S)$. Thus, the first term in (**Error! Reference source not found.**) is a standard chi-squared measure of misfit between the observed and predicted data. The second term is a positivity constraint on the amplitude parameters, p_j, with a logarithm barrier, γ [11, 12]. The logarithm term increases the gradient of the misfit if the amplitude keeps decreasing toward zero and hence ensures that solutions with negative amplitudes are avoided. A standard Levenberg-Marquardt approach is used to linearize and solve (**Error! Reference source not found.**) [7].

We also develop model selection criteria (MSC) that test if a model with $S + 1$ seamounts significantly improves the misfit relative to a model with only S seamounts. One of the applied MSC is the Unbiased Akaike Information Criterion (AIC_u) [13] defined as

$$AIC_u=\ln\left[\frac{\sum_{i=1}^{N}(V_i-R_i(\mathbf{M}_S))^2}{N_E-M}\right]+\frac{N_E+M}{N_E-M-2} \tag{6}$$

Here, we estimated the effective number of uncorrelated data, $N_E = N/C_R^2$, using the correlation pixel length, $C_R = 5$, as shown in Fig. 2. In addition, $M = 6S$ is the total number of the model parameters in $\mathbf{M}_S$. The first term in (6) is a measure of the misfit with S seamounts. However, if S is overestimated for a given dataset then AIC_u will be penalized by the second term (a measure of model complexity). Thus, $AIC_u(\mathbf{M}_{S+1})$ becomes less than $AIC_u(\mathbf{M}_S)$ if the improvement in misfit made by a model with one more seamount, $\mathbf{M}_{S+1}$, is statistically significant. The other criterion considers the F-ratio test [14], i.e.

$$F=\frac{\left[\chi^2(\mathbf{M}_S)-\chi^2(\mathbf{M}_{S+1})\right]/(M_{S+1}-M_S)}{\chi^2(\mathbf{M}_{S+1})/(N_E-M_{S+1})} \tag{7}$$

where M_S is the number of model parameters for S seamounts and the chi-squared function is the same as the first term of (**Error! Reference source not found.**). This F-statistic is tested against $P_{0.05}$ (n_1, n_2) with $n_1 = (M_{S+1} - M_S)$ and $n_2 = (N_E - M_{S+1})$, for a 90% confidence level for this study. Although both methods tend to result in the same statistical outcome, we conservatively only accept a model that passes both tests. Using the above MSC, therefore, we arrive at the number of potential seamounts that are statistically significant for the given VGG data with correlated noise.

Among the six elliptical model parameters, the misfit is most sensitive to the location and VGG amplitude of a polynomial seamount, i.e. (x_o , y_o , p). Thus, we contoured the VGG data using a 1-Eötvös interval and kept track of each contour, because seamounts produce positive gravity signals and consequently their locations and amplitudes determine the geometry of those contours. As an example (see Fig. 3), if a given area has two seamounts (the VGG peak of seamount A is larger than that of seamount B), the contouring returns the first closed polygon at the summit of seamount A. Whenever a new polygon is generated, the process estimates its area and determines a best-fit ellipse to that polygon, which usually has an irregular shape. This step parameterizes all polygons (i.e. contours) generated and enables us to recover these geometrical parameters at any contour level. As contouring proceeds, it tests if a new polygon encompasses the previous polygons. When the contouring reaches the summit of seamount B, the process results in two distinct polygons: one is from seamount A and the other is the first polygon due to seamount B. Because the latter does not include any of the previous polygons from seamount A, the contouring can recognize this event from the above test and maintain the polygon set of seamount A separately from that of seamount B, assigning unique identification numbers to each set. At each interval, we progressively construct a database of the area of a closed contour, its center location, major and minor axes, and the azimuth of the best-fit ellipse to that contour. More importantly, the contouring gives us a maximum number of potential seamounts in a given area because the first-contour of each unique polygon set is associated with a positive VGG bump that may result from an actual seamount. Thus, an initial parameter set can be constructed by using the centers (x_o , y_o) of best-fit ellipses for the first contour level, p, for each feature.

III. Results

To examine whether the new data gives us better opportunity to find seamounts, we chose near-ridge environments constrained by good bathymetry coverage (Fig. 4). The difference between VGG 16.1 (Fig. 4a) and VGG 23.1 (Fig. 4b) is noticeable in naked eyes. The VGG features due to potential seamounts are isolated more distinctly from the noisy background in VGG 23.1 than in VGG 16.1. Bathymetry data [15] also exhibit these short-wavelength underwater constructs causing vertical gravity gradient anomalies (Fig. 4c). For the given area, the nonlinear inversion method to search for small seamounts [16] is applied.

We first removed long-wavelength signals from the VGG data by applying a spatial median filter with a 300 km filter width because such regional variation is not directly associated with the seamounts themselves [17, 18]. The residual VGG grid obtained by subtracting the regional (i.e. filtered) VGG data from the original data was used for the subsequent processes.

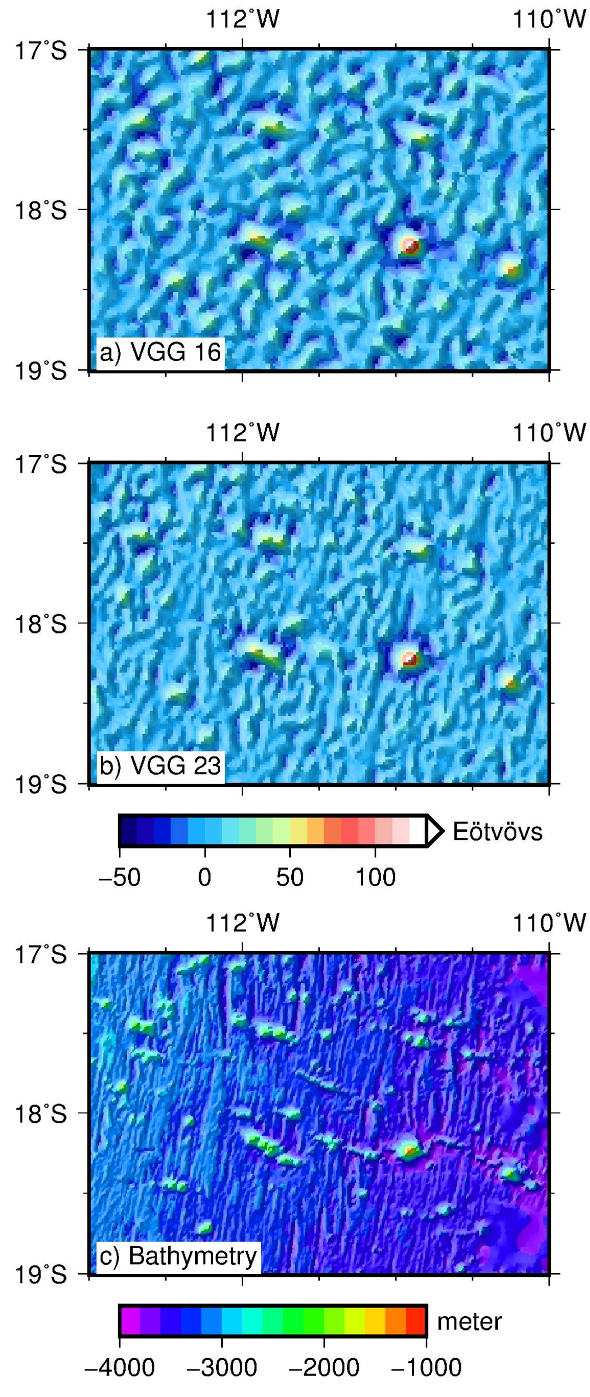

Fig. 4. Testing area located near the East-Pacific Rise, where small seamounts are present.

The initial parameters, (x_o , y_o , p), given by the slicing process are good initial choices for the location and VGG amplitude of potential seamounts (Fig. **Error! Reference source not found.**a), while the other parameters, (a, b, θ), need to be determined directly by minimizing (**Error! Reference source not found.**). However, this nonlinear system quickly becomes unstable if initial guesses for the parameters (a, b, θ) are too distant from the actual values.

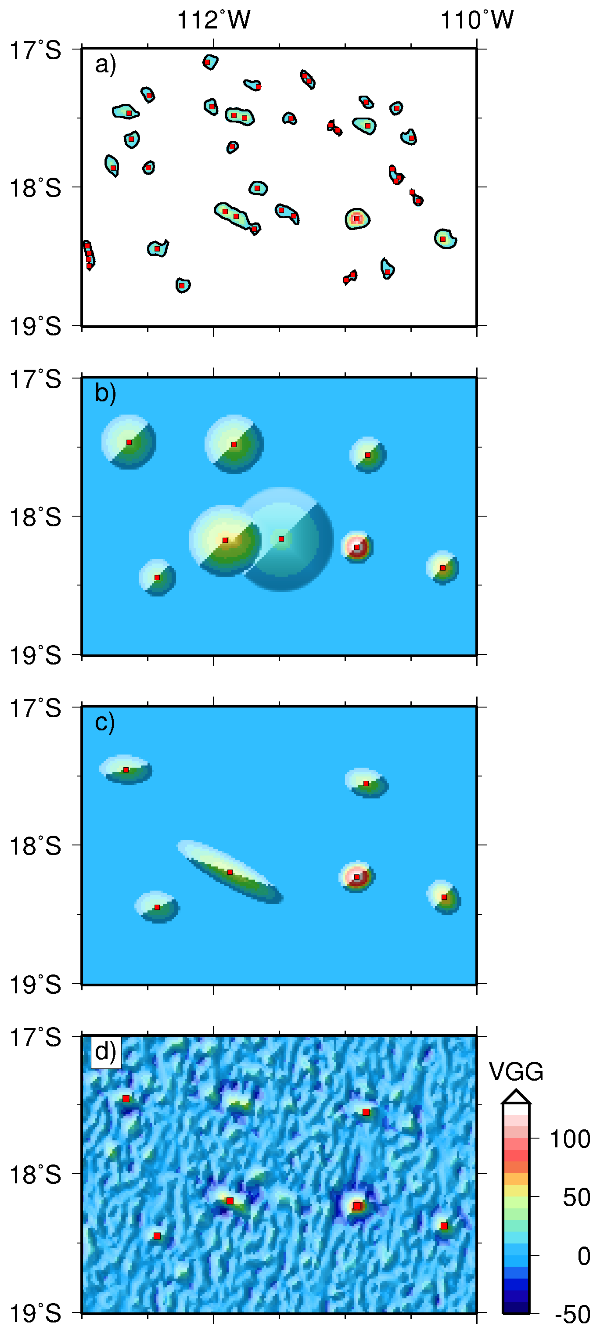

Fig. 5. Automated step-wise inversion for seamount searching. a) The initial dataset consists of the VGG data inside the base polygons and the initial model parameters, (x_o , y_o , p), prepared by contouring. The potential seamount locations are indicated by the red squares. b) Circular polynomial model. The model selection criteria (MSC) are applied to identify statistically significant potential seamounts (red squares) using the circular polynomial model. c) Elliptical polynomial model. The elliptical polynomial model is applied to approximate the given VGG data. d) The identified potential seamounts are compared with the original VGG 23.1 grid.

Thus, we constructed a step-wise inversion that solves (5) using the circular polynomial model (Fig. **Error! Reference source not found.**b) and then refines the circular parameters to yield an elliptical polynomial model (Fig. **Error! Reference source not found.**c). The detailed discussion on the automated searching processes can be seen in [16].

By comparing with the original VGG 23.1 data (Fig. 5d), the automated searching method missed about 8 potential peaks, which were removed from the list of potential peaks by the model selection criteria (Figs. 5b and 5c). Also, one elliptical seamount near 112W has the overestimated major axis as being longer than the observed. These results imply that the previously developed model selection criteria are optimized for the noisy nature of VGG 16.1 and require to be updated based on the characteristic errors of VGG 23.1. The suppressed tail of auto-covariance energy of VGG 23.1 (Fig. 2) needs more inspection to quantify its data noise. Understanding the data noise is essential to improve the non-linear inversion process and it associated statistical tests. The previously developed method appears to reject the given null hypothesis (i.e., the peaks are statistically significant) when it is true.

IV. Summary and Future Work

We utilized the vertical gravity gradient (VGG) version 23.1 derived from satellite altimetry, which includes new data from the CryoSat-2, Envisat, and Jason-1 missions, to characterize small seamounts automatically. A repeated statistical comparison for an area with no significant geologic features showed that the standard deviation of VGG 23.1 is decreased about 48% from the previous release, version 16.1, indicating the signal-to-noise ratio has been improved significantly from the previous data. In order to examine whether the new data give us better opportunities to find seamounts, we chose a near-ridge environment constrained by good bathymetry coverage. For the given area, the nonlinear inversion method to search for seamounts was applied. However, the automated searching method fail to reserve a portion of the potential seamounts during the statistical tests. These results imply that the previously developed model selection criteria were optimized for the noisy nature of VGG 16.1 and needs a major update based on the characteristic errors of VGG 23.1. Nevertheless, the new VGG data has better detectability of potential seamounts because of the improved signal-to-noise ratio. This preliminary result indicate that the VGG grid with more altimetry data sets can provide better opportunities to reveal unmapped underwater features.

Acknowledgment

The authors thank the support from the National Research Foundation of South Korea.

References

[1] H. W. Menard, *Marine Geology of the Pacific*. New York: McGraw-Hill, 1964.

[2] H. Staudigel, A. A. P. Koppers, J. W. Lavelle, T. J. Pitcher, and T. M. Shank, "Box 1: Defining the word “seamount”," *Oceanography,* vol. 23, pp. 20-21, 2010.

[3] P. Wessel, D. T. Sandwell, and S.-S. Kim, "The global seamount census," *Oceanography,* vol. 23, pp. 24-33, 2010.

[4] D. Sandwell, E. Garcia, P. Wessel, M. Chandler, and W. H. F. Smith, "Toward 1-mGal accuracy in global marine gravity from CryoSat-2, Envisat, and Jason-1," *The Leading Edge,* vol. 32, pp. 892-899, 2013.

[5] D. T. Sandwell and W. H. F. Smith, "Retracking ERS-1 altimeter waveforms for optimal gravity field recovery," *Geophys. J. Int.,* vol. 163, pp. 79-89, 2005.

[6] D. T. Sandwell and W. H. F. Smith, "Marine gravity anomaly from Geosat and ERS-1 satellite altimetry," *J. Geophys. Res.,* vol. 102, pp. 10039-10054, 1997.

[7] W. H. Press, S. A. Teukolsky, W. T. Vetterling, and B. P. Flannery, *Numerical recipes in C: the art of scientific computing*, 2nd ed. London: Cambridge Univ. Press, 1992.

[8] N. C. Mitchell, "Transition from circular to stellate forms of submarine volcanoes," *J. Geophys. Res.,* vol. 106, pp. 1987-2003, 2001.

[9] N. C. Smoot, "Guyots of the Mid-Emperor Chain mapped with multibeam sonar," *Mar. Geol.,* vol. 47, pp. 153-163, 1982.

[10] D. J. Fornari, M. R. Perfit, J. F. Allan, and R. Batiza, "Small-scale heterogeneities in depleted mantle sources: near-ridge seamount lava geochemistry and implications for mid-ocean-ridge magmatic processes," *Nature,* vol. 331, pp. 511-513, 1988.

[11] E. C. Baptista, E. A. Belati, and G. R. M. da Costa, "Logarithmic barrier-augmented Lagrangian function to the optimal power flow problem," *Electrical Power Energy Syst,* vol. 27, pp. 528-532, 2005.

[12] Y. Li and D. W. Oldenburg, "3-D inversion of magnetic data," *Geophysics,* vol. 61, pp. 394-408, 1996.

[13] C.-L. Tsai and A. D. R. McQuarrie, *Regression and time series model selection*, 1st ed. Singapore: World Scientific Publishing Co., 1999.

[14] S. Stein and R. G. Gordon, "Statistical tests of additional plate boundaried from plate motion inversions," *Earth Planet. Sci. Lett.,* vol. 69, pp. 401-412, 1984.

[15] J. J. Becker, D. T. Sandwell, W. H. F. Smith, J. Braud, B. Binder, J. Depner, *et al.*, "Global bathymetry and elevation data at 30 arc seconds resolution: SRTM30_PLUS," *Marine Geodesy,* vol. 32, pp. 355-371, 2009.

[16] S.-S. Kim and P. Wessel, "New global seamount census from altimetry-derived gravity data," *Geophys. J. Int.,* vol. 186, pp. 615-631, August 2011.

[17] W. H. F. Smith, "Marine geophysical studies of seamounts in the Pacific Ocean basin," Ph. D., Columbia Univ., 1990.

[18] P. Wessel and S. Lyons, "Distribution of large Pacific seamounts from Geosat/ERS-1: Implications for the history of intraplate volcanism," *J. Geophys. Res.,* vol. 102, pp. 22,459-22,476, 1997.